KfK 3192
Juli 1981

Preliminary Results of a Fracture Mechanics Model for Iodine-Induced Crack Growth in Zircaloy-4 Cladding Tubes at 600 and 700°C

H. Eckstein, P. Hofmann
Institut für Material- und Festkörperforschung
Projekt Nukleare Sicherheit

Kernforschungszentrum Karlsruhe

KERNFORSCHUNGSZENTRUM KARLSRUHE
Institut für Material- und Festkörperforschung
Projekt Nukleare Sicherheit

KfK 3192

Preliminary Results of a Fracture Mechanics Model for Iodine-Induced Crack Growth in Zircaloy-4 Cladding Tubes at 600 and 700°C +)

H.Eckstein, P.Hofmann

+) Paper presented at the Enlarged Halden Programme Group Meeting on "WATER REACTOR FUEL PERFORMANCE", 14th - 19th June, 1981, Hankö/Norway

Kernforschungszentrum Karlsruhe GmbH., Karlsruhe

Kernforschungszentrum Karlsruhe GmbH
ISSN 0303-4003

Summary

In the presence of iodine, the zircaloy cladding tubes may undergo low ductility failures due to stress corrosion cracking up to temperatures of about 800°C. In preflawed tubes the macroscopic plastic deformation (circumferential burst strain) is very small. The purpose of this work was therefore to investigate whether the mechanical behavior of predamaged Zircaloy-4 cladding at 600 and 700°C can be described using fracture mechanics. It is evident from the studies that the stress intensity concept of linear-elastic fracture mechanics (LEFM) is suitable to describe the material behavior. Mathematical description of the crack growth by LEFM methods is intended to estimate critical material conditions which can lead to cladding failure and the expected time-to-failure.

Vorläufige Ergebnisse eines bruchmechanischen Modells zur Beschreibung des jodinduzierten Rißwachstums in Zircaloy-4-Hüllrohren bei 600 und 700°C

Zusammenfassung

In Gegenwart von Jod kann es bei Temperaturen bis etwa 800°C zum verformungsarmen Versagen von LWR Hüllrohren infolge Spannungsrißkorrosion kommen. Besonders bei vorgekerbten Rohren ist die makroskopische, plastische Verformung (Umfangsdehnung) sehr klein. Im Rahmen dieser Arbeit sollte daher untersucht werden, ob das mechanische Verhalten von vorgeschädigten Zircaloy-Hüllrohren bei 600 und 700°C mittels bruchmechanischer Methoden beschrieben werden kann. Wie diese Untersuchungen zeigen, erweist sich das Spannungsintensitäts (K_I)-Konzept der linear elastischen Bruchmechanik (LEBM) zur Beschreibung des Materialverhaltens als geeignet. Die mathematische Beschreibung des Versagensmechanismus mit den Methoden der LEBM hat zum Ziel, kritische Materialzustände, die zum Versagen der Hüllrohre führen, sowie die zu erwartende Standzeit abzuschätzen.

Contents

1. Introduction

It is a generally established fact that zircaloy cladding can fail as a result of stress corrosion cracking (SCC) when the power is increased too quickly in light-water cooled reactors (LWR). The prerequisites for SCC are the combined impact of mechanical tensile stress (caused by mechanical interaction between fuel and cladding) and chemical attack of the cladding inner surface, primarily by the volatile fission product iodine. These conditions may exist during power increases in normal operation, but may also occur during reactor incidents as a result of mechanical interaction between fuel and cladding as in an "Anticipated Transient without Scram" (ATWS), "Reactivity Initiaded Accident" (RIA), or as a result of the difference between system and internal rod pressures as in a "Loss of Coolant Accident" (LOCA).

Investigations conducted worldwide up to the present time have been limited to the study of SCC behavior of zircaloy (Zry) cladding under normal reactor operating conditions (up to 500°C maximum). Various fracture mechanics models have been developed which describe initiation and propagation of stress corrosion cracks under normal operating conditions. The purpose of the models is to evaluate the critical values of stress, stress intensity, deformation, and iodine concentration as function of temperature, which can lead to cladding failure. Studies on the possibility of describing SCC of zircaloy cladding at temperatures above 500°C using fracture mechanics are presented in this paper.

2. Selection of an Appropriate LEFM Model

General aspects of fracture mechanics, various model concepts used to describe zircaloy burst behavior, and selection and discussion of the model used in this work are described in the following sections.

2.1 General Aspects of Fracture Mechanics

The Griffith model of cracks is the basis of a static and dynamic description of crack behavior /1/. It assumes an elliptical hole in an elastic disk of infinite dimensions under uniaxial tensile stress. For a long narrow gap, the assumption is made that the elliptical hole has developed into a slit whose minor axis has disappeared. Unfortunately, the calculated stresses at the crack tips are infinite in this case /2,3/, due to mathematical singularities which arise at these points (the bending radius is not defined at the crack tips). Since this is physically impossible, approximative expressions are applied to the immediate environment of the crack tip. G.I.Barenblatt avoided this problem by taking into account molecular cohesive forces which exist at the crack tips to describe the stresses at these points /1/. These cohesive forces cause smooth closure of the crack surfaces(the opening angle between the fracture surfaces is zero at the crack tip). The distribution of stresses along the plane of propagation ahead of a crack in a body under any load is obtained from the superposition of a normal elastic stress condition (according to Griffith, without considering the cohesive forces) and a stress condition originating exclusively from the cohesive forces.

Linear-elastic crack models are not sufficiently exact to describe the crack behavior of ductile materials. Appropriate elastic-plastic solutions must be found to calculate the stresses and strains around the crack tip, where plastic creep occurs (particularly in metals). These solutions must account for phenomena in the plastic zone as functions of the load and the material properties. This has been done in the model proposed by D.S. Dugdale /1/. He treats the plastic zone preceding the crack tip as an elongation of the actual crack. Within this narrow region of plastic deformation, the material undergoes a constant yield stress σ_F; and outside the plastic zone the material exhibits strictly elastic behavior.

If the deformed area at the crack tip is small, the stress and deformation fields of the crack can still be described - similar to the

linear elastic models - by the stress-intensity factor K_I introduced by G.I.Irwin /4,5/, since the elastic behavior of the specimen as a whole is insignificantly influenced /6/. Minor deviations from linearity can then be incorporated by suitable treating the plastic zone as an extension of the actual crack. If the deviations from linearity are very large, this phenomenon (termed elastic-plastic fracture mechanics) and the occurrence of fracture must be described by other parameters independent of the specimen geometry and the loading. The two most advanced methods of elastic-plastic fracture mechanics are the Crack-Opening Displacement Concept (COD) and the J-Integral method /7,8/.

2.2 Model Concepts for Burst Tests of Zircaloy Cladding

In the literature, the K_I-concept of linear elastic fracture mechanics (LEFM) is widely used to describe Zry cladding fracture due to iodine-induced SCC at normal reactor operating temperatures ($\leq 330^{\circ}C$) /9/. SCC of Zry under the influence of iodine has been intensively studied by Tucker, Kreyns and Kearns /10/, who used an LEFM model according to Kreyns et al./11/. From isothermal, isobaric experiments (unirradiated Zry cladding, internally prenotched, internal pressure applied, temperature $<400^{\circ}C$), time-to-failure was determined as a function of mean hoop stress, temperature and initial iodine concentration.

Effort have been made recently to include a plastic deformation zone and the influence of cohesive forces between atoms in the area ahead of the crack tip, in a realistic crack model /12/. Using elastic-plastic fracture mechanics, E.Smith and A.K.Miller /13,14/ developed a theoretical model describing transcrystalline SCC in irradiated Zry-4, taking into account a plastic deformation zone and cohesive forces.

2.3 Selection of Model

A modified LEFM model was used as the basis of our own investigations conducted at temperatures higher than under normal reactor operating conditions. Since low-ductility (brittle) failure of Zry due to iodine is observed up to about $800^{\circ}C$, especially for mechanically prenotched

cladding specimens /15/, predominantly elastic material behavior can be expected. However, the Zry cladding material at the tip of the crack behaves as an elastic-plastic material, which results in formation of a small plastically deformed zone. The stress intensity in front of the crack tip is given by J.C. Newman and I.S.Raju /16,17/, since the geometry parameter introduced there describes rather well the conditions encountered in SCC experiments with Zry cladding (a tube loaded by internal pressure containing a semi-elliptical axial crack on its inner wall). Plastic deformation ahead of the crack tip is taken into account using the concepts of D.Munz /18/. Mathematical description of this failure mechanism by LEFM methods eventually should result in statements concerning critical material conditions leading to cladding bursting as well as in statements concerning the times-to-failure anticipated for familiar load cases.

2.4 Discussion of Model

If a Zry cladding specimen containing a defined amount of iodine is loaded by constant internal pressure so that the nominal stress σ_n does not exceed the yield stress $\sigma_F = (\sigma_{0.2} + \sigma_B)/2$, a distinction must be made between the three phases of the SCC failure mechanism: (a) incubation, (b) crack growth, and (c) rupture of the fracture residual area.

2.4.1 Incubation

The incubation time (t_I) is dependent on the loading and on the degree and geometry of predamaging (whether it occurred during the fabrication process or was applied mechanically). At the end of the incubation phase, an intercrystalline incipient crack has just been formed ahead of the flaw as a result of the combination of initial stress intensity $K_{I,O}$ at this point and the corrosive action of iodine.

2.4.2 Crack Growth

Given that the original depth of the flaw and the incipient crack is a_o, the crack depth increases according to the law /1/

$$\frac{da}{dt} = C \cdot K_I^n \quad , \tag{1}$$

where C and n are experimentally determined constants. The stress intensity K_I at the crack tip increases with increasing crack depth according to

$$K_I = \sigma_n \sqrt{\pi a}\, Y_{(a)} \quad , \tag{2}$$

where the function Y (a) takes into account the geometry of the crack front and the size of the crack with respect to the wall thickness.

Elongation of the plastically deformed zone formed ahead of the crack front (in the direction of crack growth) is expressed by /18/

$$\omega = \frac{2}{\beta \pi} \left(\frac{K_I}{\sigma_F}\right)^2 \quad . \tag{3}$$

If a condition of plane-stress in the thin-walled cladding tubes is assumed ahead of the crack front, then $\beta = 2$. As an approximation for the model an effective crack is then defined whose tip lies in the middle of the plastic zone, so that it has the length

$$a_{eff} = a + \frac{1}{\beta \pi} \left(\frac{K_I}{\sigma_F}\right)^2 \quad . \tag{4}$$

This gives an effective stress intensity for the K_I-model, using an effective geometry function, of

$$K_{I,eff} = \sigma_n \sqrt{\pi\, a_{eff}}\, Y_{(a_{eff})} \quad . \tag{5}$$

The real crack grows until it attains a critical depth a_c. This critical depth is not determined by the LEFM. However, if the plastic threshold

load $\sigma_{net,c}$ is reached in the remaining wall thickness, it is assumed that an instability occurs in the crack growth. The relationship between the yield stress σ_F, the load in the remaining wall thickness σ_{net}, and the crack depth is determined by

$$\sigma_{net} = \sigma_F / M^x \quad . \tag{6.1}$$

For continous surface cracks M^x is derived using the FOLIAS-Factor M, which considers local changes in tube geometry in front of the crack tip /19,20/

$$M^{**} = \frac{1 - \frac{a}{M \cdot w}}{1 - \frac{a}{w}} \tag{6.2}$$

with

$$M = [1 + 1{,}255\ \rho^2 - 0{,}0135\ \rho^4]^{1/2} \tag{7}$$

and

$$\rho = \frac{\P\, c}{4\sqrt{R_i w}}$$

where R_i is the tube inner radius, w the wall thickness, and c is half the crack length.

The critical crack depth a_c can therefore be defined as the point at which crack growth becomes unstable (plastic breakoff criterion). From equations 6 and 7 follow

$$a_c = w \frac{\sigma_F - \sigma_{net,c}}{\frac{\sigma_F}{M} - \sigma_{net,c}} \tag{8.1}$$

where for thin walled tubes /19/

$$\sigma_{net,c} = p_B \frac{R_i + a_c}{w} \tag{8.2}$$

where p_B is the burst pressure.

2.4.3 Rupture of Fracture Residual Area

As soon as the critical crack depth a_c is attained, Eq. 1 becomes invalid and spontaneous rupturing of the fracture residual area occurs. This rupturing takes place so quickly that no time portion is calculated for it in the model.

The total time-to-failure (t_B) is thus composed

$$t_B = t_I + t_R \tag{9}$$

where t_I is the incubation time and t_R is the crack growth time.

The incubation time (t_I) is a function of the depth and geometry of the notch, and the applied load. It can be written

$$t_I = A \cdot F\,(a_{eff,o},\ Y_{(a_{eff,o})},\ \sigma_n) \tag{10}$$

where A is a constant.

The crack growth time (t_R) can be calculated by integrating Eq. 1 within the limits a_o and a_c to obtain

$$t_R = \frac{1}{C\,\sigma_n^n\,\pi^{n/2}} \int_{a_o}^{a_c} \frac{da}{a_{eff}^{n/2}\,Y_{(a_{eff})}^{n}} \tag{11}$$

One method of determining whether this model is suitable for describing material failure is to measure the degree of agreement between the experimental time-to-failure (t_M) and the calculated time-to-failure (t_B). Another indication of agreement is whether the crack growth law (Eq. 1) with equal values of the constants C and n, applies to all cases independent of the load, extent of predamage, and stress intensity.

3. Experiment Description

The experimental program and the experiment conduct are briefly described in the following sections.

3.1 Experimental Program

The relationship between the effective stress intensity and the rate of crack propagation can be represented using Eq. 1

$$\frac{da}{dt} = C \cdot K_{I,eff}^{n} \qquad (12)$$

C and n are constant for fixed environmental conditions (temperature and iodine concentration). Since crack propagation cannot be followed exactly during the experiments, the variables (da/dt) and $K_{I,eff}$ are assumed to be values averaged over the duration of the experiment. Moreover, the initial value $K_{I,eff,o}$ can be determined from the initial geometry of the crack (a_o) and the stress applied (σ_n). This means that two defined values of the stress intensity are available: (a) $K_{I,eff,o}$, which determines the time of crack formation and the starting velocity of stable crack growth; and (b) $K_{I,eff,c}$, which corresponds to a critical crack depth (a_c) at which crack propagation becomes unstable, i.e., the critical threshold strength of the material is reached in the fractional residual area.

The test program was organized so that under isothermal test conditions

1. a variation of stress intensity was possible by varying the internal pressure of the cladding without changing the initial geometry a_o of the mechanically produced internal notch; or
2. a variation of the average crack velocity (da/dt) with respect to the effective stress intensity $K_{I,eff}$ was attained by varying the initial crack depth without changing the time-to-failure (by applying different pressures).

The test program was intended to verify the validity of the K_I concept for iodine-induced SCC of Zry-4 cladding at elevated temperatures (600 and 700°C).

3.2 Experiment Conduct

Isothermal, isobaric burst experiments were performed at the ROBERTA

facility to study iodine-induced stress corrosion cracking of Zry-4 cladding at 700 and 600°C in helium. As-received and preflawed tube specimens with varying notch depths were used. The specimens were about 100 mm long, with an outer diameter of 10.76 mm and a wall thickness of 0.72 mm. The times-to-failure varied between 5 and 3600 s for internal pressures between 50 and 260 bar. The iodine concentration was 10 mg/cm^3 in all experiments. The construction of the burst apparatus and the experiment conduct are described in /15/.

4. Test results and Discussion

In general, three types of cladding failure must be distinguished in performing and interpreting iodine-induced SCC burst test:

1. The average stress in the residual cross section is initially so high that it equals the ultimate yield strength. This results in spontaneous failure even if the stress concentration ahead of the crack tip is not taken into account. It is possible that the deformation rate is so high that iodine cannot be supplied quickly enough to the crack tip, and failure is completely ductile. That is, failure is independent of the SCC mechanism.

2. The stress distribution in the residual cross section is such that a zone of plastic deformation is formed ahead of the crack front and the stress intensity is smaller than $K_{I,eff,c}$. Iodine reacts aggressively with the zircaloy, and the material shows brittle rupturing behavior with very little strain. That is, failure is SCC-dependent. Crack growth can be described using modified linear-elastic fracture mechanics.

3. The stress in the residual cross section is less than a given lower limit below which zircaloy cladding failure (within certain time limits) can no longer be attributed unequivocally to SCC. Creep processes dominate strain behavior. Application of linear-elastic fracture mechanics (even taking into account the plastic zones) is not longer possible.

Material behavior and SEM examinations are discussed for the tests conducted at 600 and 700°C, with respect to these three failure types, and specific fracture mechanics calculations are described in the following sections.

4.1 Material Behavior at 700°C

Results obtained at 700°C are shown in Figures 1,2, and 3. These results correspond to failure type 2. In Figure 1 note, that as the time-to-failure increases, the influence of the notches decreases. Apparently, a minimum pressure exists (corresponding to the lower limit stress) below which the influence of both iodine and predamaging is no longer effective (failure type 3). The load(internal pressure) is so small that the necessary critical cladding tube stress required for SCC is probably not produced. In Figure 2 it is apparent that the strain increases with the deformation rate after passing through a minimum [+)], and that, at high strain rates, the influence of different types of predamaging is negligible. The strains in the range of higher pressures (p_B > 70 bar) were very low for all of the predamaged cladding (<5%), as shown in Figure 3. It is probable that, for high pressures and short times-to-failure, cladding stress is so large that the ultimate tensile strength of the material is quickly reached and the time available for crack formation, crack propagation, and iodine-zircaloy reaction is very short (failure type 1).

4.2 Material Behavior at 600°C

As at 700°C, burst pressure decreases with increasing time-to- failure, but the pressures are higher overall (Figure 4). The influence of

---

+) The mean deformation rate indicated in Figure 2 (which is not directly related here to the velocity of crack propagation) is very inaccurate for describing material behavior because it may deviate by several orders of magnitude from the instantaneous deformation rate.

small notches (up to 100 µm) is largely reduced up to a time-to-failure of about 10^4 s; greater predamaging seems to be not negligible even with very large times-to-failure. The dependence of burst strain on internal pressure is much more pronounced at 600°C than at 700°C (Figure 5). For the He reference specimens, a clear strain maximum of about 70% can be seen at about 170 bar. The predamaged specimens appear to have a strain maximum of approximately 13% which is displaced towards lower pressures as the notch depth increases, and is preceded at higher pressures by a strain minimum. But a definite statement about this behavior will be possible only after additional tests have been performed at pressures up to 250 bar. The as-received specimens tested with iodine did not show the same behavior as the predamaged specimens. A continuous reduction in burst-strain was observed with increasing pressure. The relationship between burst strain and average deformation rate in Figure 6 is similar to the results obtained at 700°C. A minimum of 2 to 5% strain is clearly visible for the predamaged specimens. However, the subsequent increase in burst strain shows almost no difference between the curves for 100, 150 and 200 µm notches. The burst strains probably decrease again with increasing strain rate (i.e., with increasing pressure) and approach the descending portion of the as-received He reference specimen curve for long times-to-failure.

4.3 Scanning Electron Microscope Examinations (700°C)

As-received and predamaged specimens containing iodine were examined with the scanning electron microscope (SEM). The photographs showed that, at 700°C, both microscopic and macroscopic axial intercrystalline incipient cracks had formed over the entire cladding inside surface (Figure 7). The cracks varied in depth and only one crack led to failure. In the as-received specimens, the incipient crack resulting in failure was that in which the grain boundaries were suitably located ahead of the crack front so that crack growth was fastest due to a sufficiently high stress intensity. In the predamaged specimens SCC differed in that the notches, which are deeper than the damage caused during manufacturing (pitches, grooves), defined the points at which

the stress intensity is both higher and initially known. However, axial intercrystalline incipient cracks also formed over the entire inside surface in the predamaged cladding. SEM examinations further showed that nearly the whole fracture surface was intercrystalline in character (Figure 7). Only in a few specimens could an indication of transcrystalline fracture be observed. Clearly ductile residual fracture surfaces, which would be expected if the stress in the residual cross section attained the ultimate strength, did not occur. This means that the cracks were intercrystalline and propagated beyond the critical crack depths predicted by the model. An explanation for this behavior is that at 700°C, iodine significantly reduces the stability of the grain boundary so that spontaneous fracture takes place along the grain boundaries when a critical strength is reached. Iodine therefore exerts a considerable and, moreover, quick depth effect. Near the fracture surfaces (within several grain diameters), individual grains were observed in some places to be only loosely held together, which supports this explanation.

4.4 Scanning Electron Microscope Examinations (600°C)

The appearance of the cladding inside surface in the as-received and predamaged specimens at 600°C was not similar to that of the specimens tested at 700°C. The predamaged specimens exhibited very few or no microscopic incipient cracks; the cladding inside appeared to be insensitive to iodine-induced SCC away from the notches compared to the behavior at 700°C. The as-received specimens also exhibited very few incipient cracks.

The rupture surface geometries depended on the initial notch depths. For small notches (about 50 µm deep and 5000 µm long) the crack front first extended radially to the cladding midwall, and continued to grow elliptically until failure occurred (Figure 8a). For average notch depths (about 100 µm and 10^4 µm long), the geometry of the fracture surface varied (Figure 8b). Crack growth as described above for small flaws, a M-shaped facture surface, and a continuous semi-elliptical crack front, were observed. For large notch depths (about 200 µm and

2 mm long), all of the crack fronts were semi-elliptical (Figure 8c). Different locations of the maximum stress intensity can explain these different fracture surface geometries. The axial crack length increases if the maximum stress intensity occurs at the axial ends of the crack front. In contrast, if the maximum stress intensity lies at the axial middle of the crack front, the crack propagates as a semi-ellipsoid.

To depth of 75 to 90% of the wall thickness, the fracture surfaces at 600°C were intercrystalline in character (Figure 9). In about half the specimens, this region was followed by a transcrystalline fracture extending either to the outside surface or to a point at which ductile residual fracture occurred. The fracture type and the extend of the intercrystalline crack path could not be differentiated for all of the specimens because of a thick coating (zircaloy-iodine reaction product) on the fracture surfaces.

4.5 Fracture Mechanics Calculations

The computation methods, which initially included the simplification of an incubation time equal to zero, and a discussion of the results are presented in the following sections.

4.5.1 Computation Methods

Initial fracture mechanics calculations have been made for the experiments performed at 600 and 700°C. It was assumed for simplification that the crack growth law (Eq. 1) can be applied to the entire time-to-failure (setting the incubation time $t_I = 0$). That is, the crack growth time t_R calculated in the model (from Eq. 11) is set equal to the total time-to-failure t_M measured in the experiment. C and n can therefore be determined iteratively since all the other variables $(t_B, a_o, a_c, Y_{(a_{eff})})$ can be measured or calculated. The iterative method, performed separately for each temperature, is divided into the following sections:

1. A value is fixed in advance for the exponent n (the same for all experiments) and for each individual test i the corresponding C_i

is calculated from Eq. 11.

2. The value of n is optimized until scattering of the C_i-values around a (logarithmic) mean value C_m reaches a minimum.

3. Using the optimum pairs of values (C_i and n) for each test a corresponding value for (da/dt) is determined for each $K_{I,eff,o}$ and $K_{I,eff,c}$.

4. At a given temperature, the pair of values (C_m and n) determines the line log (da/dt) versus log ($K_{I,eff}$) (Figures 10 and 11). The equation

$$\frac{da}{dt} = C_m \cdot K_{I,eff}^n$$

thus constitutes an approximation to the desired crack growth relationship.

5. The measured and calculated times-to-failure are then compared by calculating t_B for each test from the pair of values (C_m and n) and Eq. 11, and plotting it versus t_M (Figures 12 and 13).

4.5.2 Discussion of Results

The modified LEFM model already shows promising indications of the usefulness even in a first approximation (incubation time $t_I = 0$). The da/dt versus $K_{I,eff}$ diagram at 600°C (Figure 10) shows a rather good agreement with the model. The scatter is probably a result of inaccurate determination of crack velocity since the incubation period (which depends on the initial crack depth a_o) has not been taken into account. The considerable scatter in the comparison between measured and calculated times-to-failure at 600°C probably has the same systematic cause (Figure 12). The results at 700°C are similar, with more scatter than at 600°C. Calculations which include the incubation period will show whether application of the modified LEFM model is restricted at 700°C.

5. Conclusions

- Iodine in as-received Zircaloy-4 cladding leads to low ductility failure as compared with He reference specimens. Burst strain is further decreased in predamaged specimens. Zircaloy shows "brittle" fracture behavior in the presence of iodine.

- Macroscopic plastic deformation of predamaged tube specimens depends on temperature, burst pressure and initial crack depths. At 700°C, measureable plastic deformation was similar to that at 600°C. Burst strain depended on the average deformation rate. For deformation rates between 10^{-3} and 10^{-4} (1/s) at 600 and 700°C, minimum strains occurred (<5%) on the initial notch depth.

- Due to the "brittle" behavior of Zircaloy-4 in the presence of iodine, it is possible to describe cladding mechanical behavior using a modified K_I concept of linear-elastic fracture mechanics (LEFM). The agreement between measured and theoretically determined times-to-failure was better at 600 than at 700°C. The applicability of LEFM may be restricted at 700°C. This must be clarified by further studies.

- The behavior of tubes with cracks can be described by the equation $da/dt = C \cdot K^n$, by considering and correcting for the plastic region in front of the crack tip. At 600°C the stress intensity factor varied between 1 and 8 $MPa \cdot m^{0.5}$ for average crack velocities of 10^{-4} m/s to 10^{-1} m/s; and at 700°C it varied between 0.8 and 3 $MPa \cdot m^{0.5}$ for average crack velocities between 10^{-5} and 10 m/s. Scattering in the results might be reduced when the incubation period is included in the determination of C and n.

- Crack development at 700°C was noticeably different than at 600°C. At 700°C, the cracks were nearly fully intercrystalline; no residual fracture or a very small ductile residual fracture was observed. At 600°C, the cracks were intercrystalline to a depth of 75 to 90% of the wall thickness, followed by a transcrystalline transition region

before ductile residual fracture occured. The fracture shape depended on the depth of the initial notch at 600°C but not at 700°C.

At 700°C, material failure occurs by grain boundary rupture due to chemical corrosion ahead of the crack. This type of failure is not dependent on crack propagation and is therefore spontaneous. Consequently, less local plastic deformation takes place at 700°C than at 600°C, where ductile residual fractures accompanied by void formation were generally observed.

6. Acknowledgements

The authors are grateful to Prof. Dr. W. Dienst and Prof. Dr. D. Munz for many stimulating technical discussions and Mrs. Deborah Kerwin for the critical suggestions during the preparation of this paper. They are also indebted to Mr. J. Burbach for the SEM studies and Mr. H. Metzger for the metallographic examinations.

7. Literature

/1/ H.G. Hahn
Spannungsverteilung von Rissen in festen Körpern,
VDI-Forschungsheft 542 (1970), VDI-Verlag Düsseldorf

/2/ N.I. Mus'chelishvili
Some basic problems of the mathematical theory of elasticity,
P. Noordhoff Ltd., Groningen (1953)

/3/ G.V. Kolosov
Über die Anwendung der komplexen Funktionstheorie auf das ebene Problem der mathematischen Elastizitätstheorie
(Original russisch)
Dissertation Universität Yuriew (Dorpat) (1909)

/4/ G.R. Irwin, J.A. Kies
Fracturing and fracture dynamics
Welding J., 31 (1952), Research Suppl., S-95-100 s

/5/ G.R. Irwin
Relation of stress near a crack to the crack extension force,
Actes 9th congr. Intern. Mec. Appl. Bruxelles 1956,
Bruxelles, Université de Bruxelles (1957), Bd.8, S.245-251

/6/ K.H. Schwalbe
Bruchkriterien der Bruchmechanik,
Fortschritts-Bericht VDI-Z Reihe 18, No.3 (1977)

/7/ J.R. Rice
A path independent integral and the approximate analysis of strain concentration by notches and cracks
Brown Univers. Providence, Div. of Engng, Report E 39,
ARPA SD-86 (1967)

/8/ Merkle, Corten
A J-Integral analysis for the compact specimen, considering axial force as well as bending effects, Transactions of the ASME (1974)
Journal of Pressure Vessel Technology, 96 (1974), pp. 286-292

/9/ EPRI-NASA Cooperative Project in stress corrosion cracking of Zircaloys,
EPRI-NP 717, Project 455-1, Final Report, Section 5 (March 1978)

/10/ R.P. Tucker, P.H. Kreyns, J.J. Kearns
The effects of internal surface flaws, iodine concentration and temperature on the stress corrosion cracking behaviour of Zry-4 tubing,
WAPD-TM-1248 (1976)

/11/ P.H. Kreyns, G.L. Spahr, J.E. McCauley
An analysis of iodine stress corrosion cracking of Zry,
J.N.M. 61 (1976), S. 203-212

/12/ A. Garlick, J.G. Gravenor
A Criterion and Mechanism for Power Ramp Defects,
AED-Conf. 1977 (667-000), ANS Topical Meeting in Water Reactor Fuel Performance, St. Charles, III., May 1979

/13/ E. Smith, A.K. Miller
Stress corrosion fracture of Zircaloy cladding in fuel rods subjected to power increases. A model for crack propagation and the Failure threshold stress.
J.N.M. 80 (1979), S. 291-302

/14/ J.T.A. Roberts et al.
A SCC model for pellet-cladding-interaction failures in LWR fuel rods,
4th Intern. Conf. on Zirconium in the Nucl. Industry, Stratford-upon-Avon (1978), ASTM-STP 681

/15/ P. Hofmann
Einfluß des Spaltproduktelementes Jod auf das Verformungs- und Bruchverhalten von Zry-4 Hüllrohren bei Temperaturen zwischen 600 und 1000°C,
KfK 2661 (1978)

/16/ J.C. Newman, I.S. Raju
Stress Analysis and Fracture of Surface Cracks in Cylindrical Pressure Vessels,
5. SMIRT-Conf., Vortrag G7/3, Berlin 1979

/17/ I.S. Raju, J.C. Newman
Stress Intensity Factors for a wide range of semi-elliptical surface cracks in finite thickness plates,
Eng. Fracture Mech. 11, 817-829, 1979

/18/ D. Munz
Linear-elastische und elastisch-plastische Bruchmechanik ...,
DFVLR-Forschungsbericht 79-31, 1979

/19/ J.F. Kiefner, W.A. Maxey, R.J. Eiber, A.R. Duffy
Failure Stress Levels in Pressurized Cylinders,
ASTM-STP 536, 1973, S.461-481

/20/ H.D. Schulze, G. Togler, E.Bodmann
Fracture mechanics analysis on the initiation and propagation of circumferential and longitudinal cracks in straight pipes and pipe bends,
Nucl. Engineer. and Design 58 (1980) 19-31

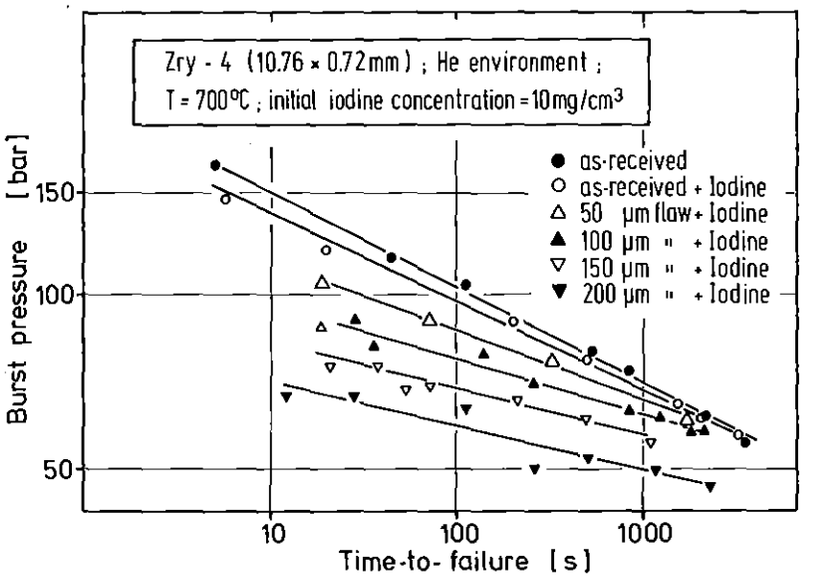

Fig.1: Time-to-failure of as-received and preflawed Zircaloy-4 tubing at 700°C in He (for specimens with and without iodine).

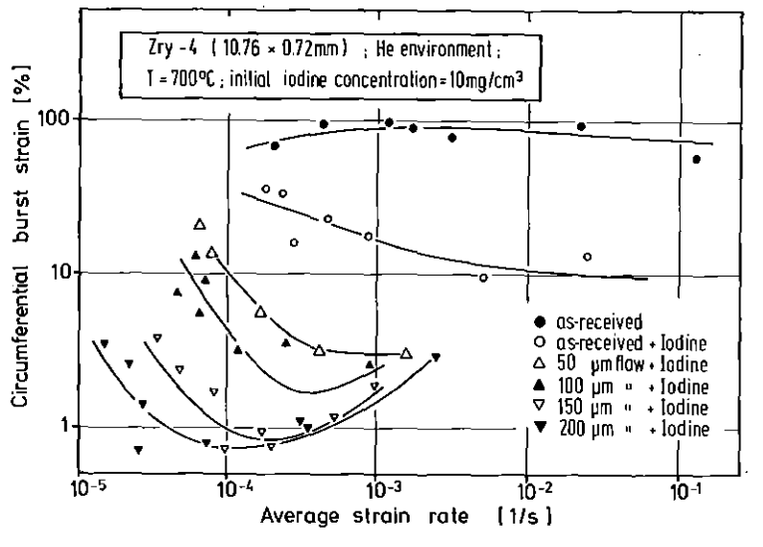

Fig.2: Circumferential burst strain versus deformation rate of Zircaloy-4 tubing at 700°C.

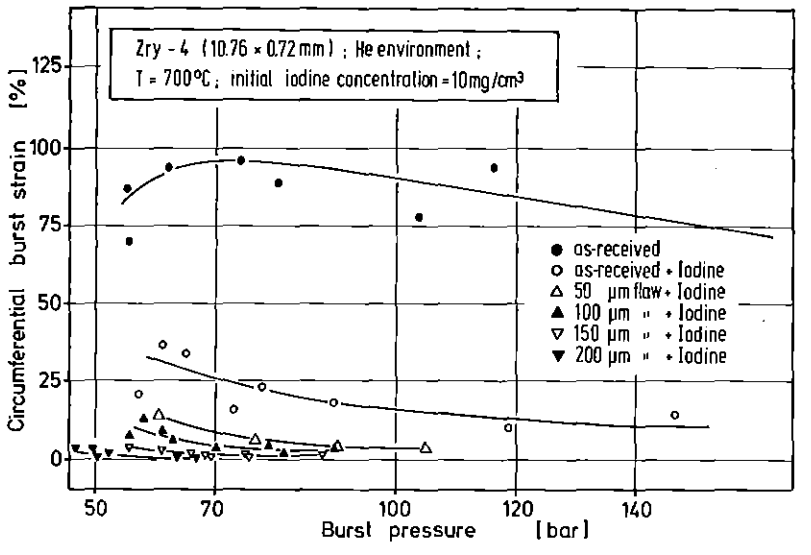

Fig.3: Circumferential burst strain versus pressure of Zircaloy-4 tubing at 700°C.

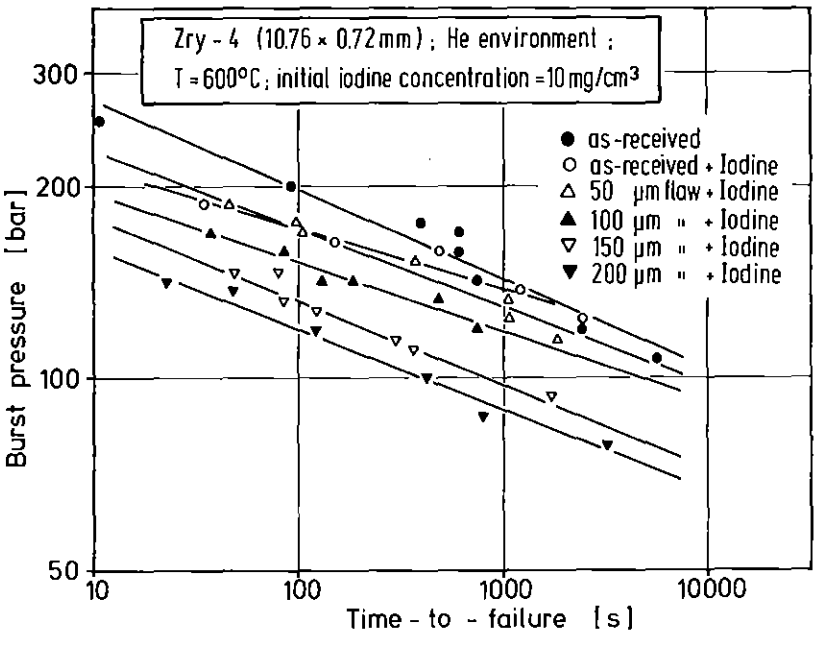

Fig.4: Time-to-failure of as-received and preflawed Zircaloy-4 tubing at 600°C in He (for specimens with and without iodine).

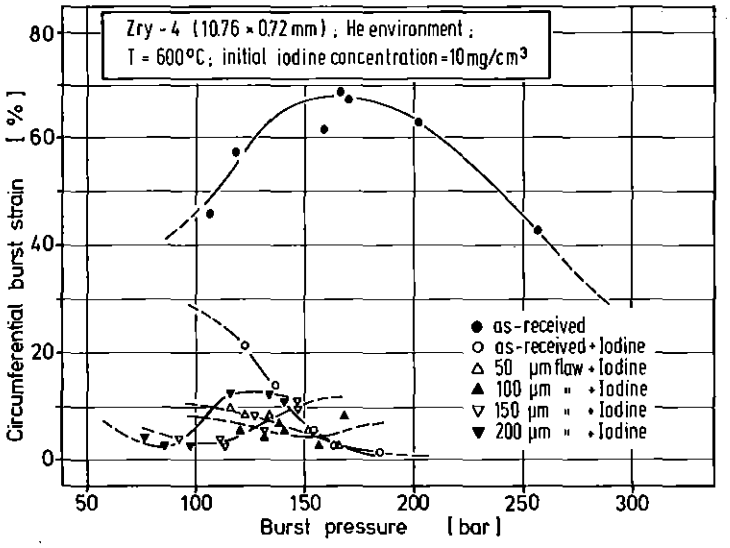

Fig.5: Circumferential burst strain versus pressure of Zircaloy-4 tubing at 600°C.

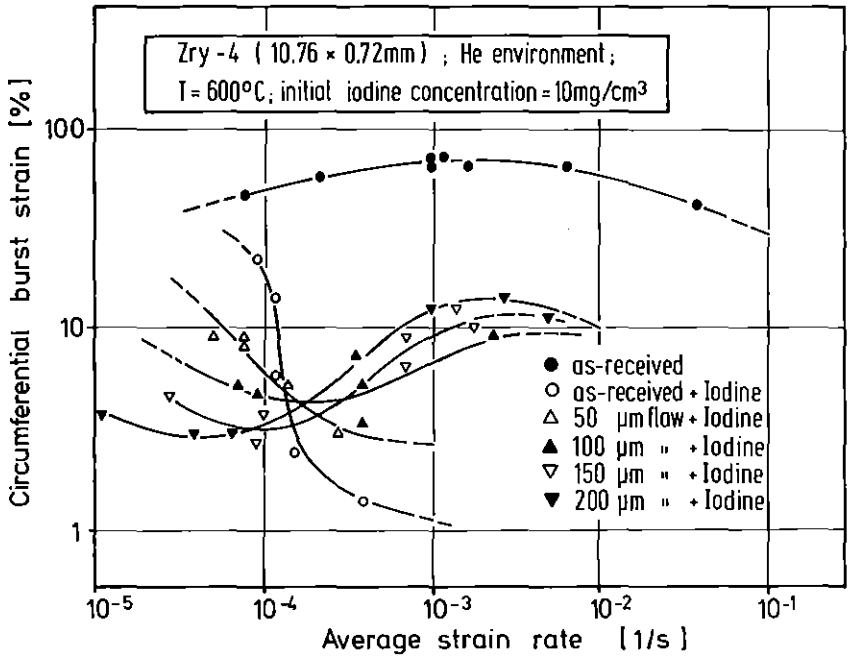

Fig.6: Circumferential burst strain versus deformation rate of Zircaloy-4 tubing at 600°C.

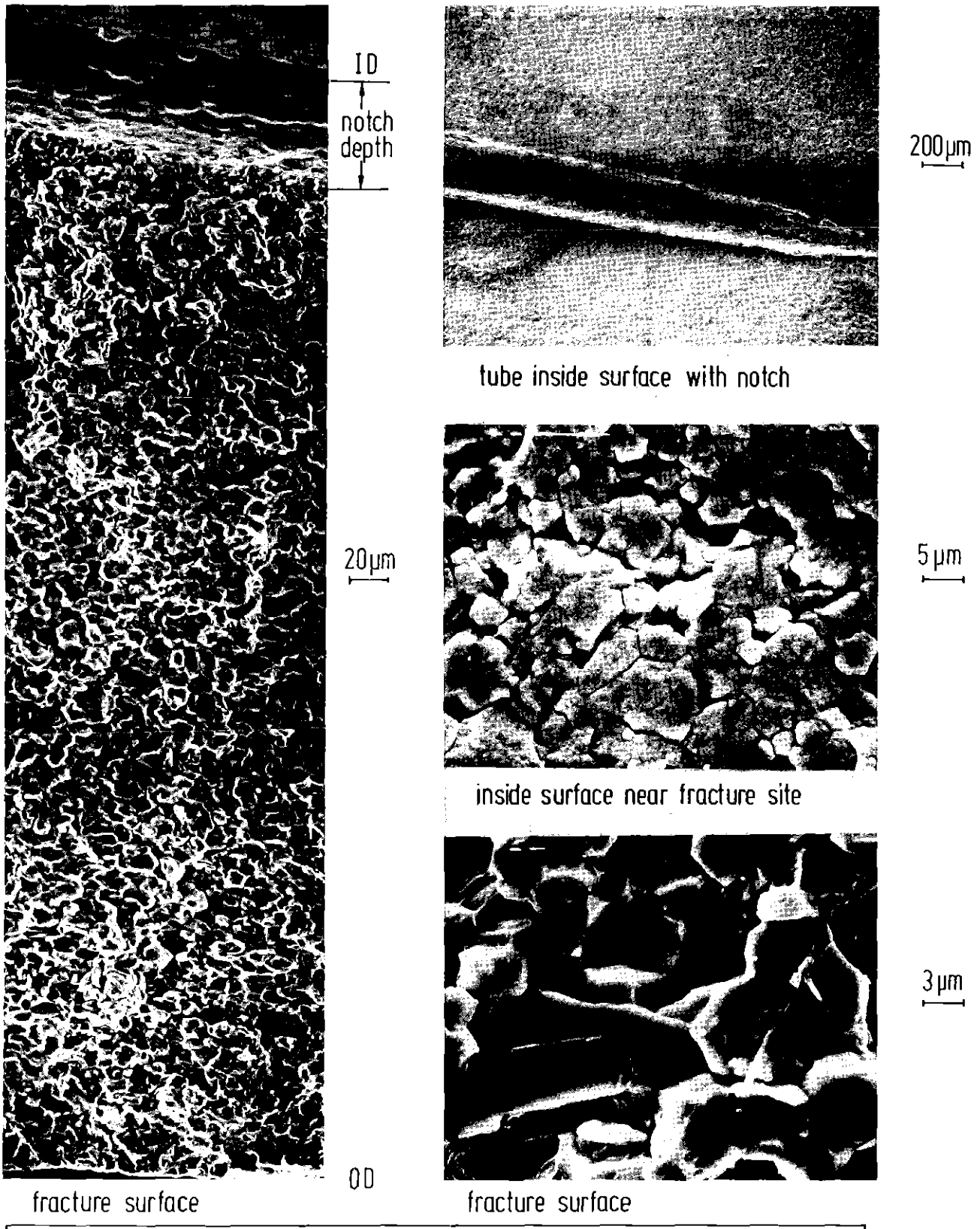

Fig.7: Zircaloy cladding tube inside surface and fracture surface after failure under helium-iodine gas pressurization at 700°C.

SEM - EXAMINATIONS

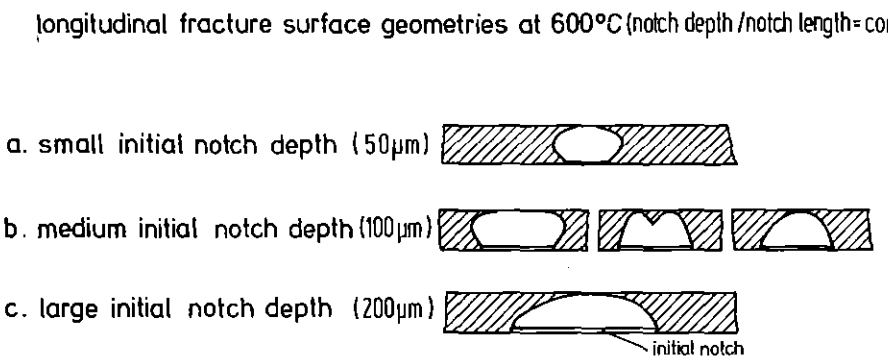

Fig.8: Longitudinal fracture surface geometries at 600°C for different initial notch depths.

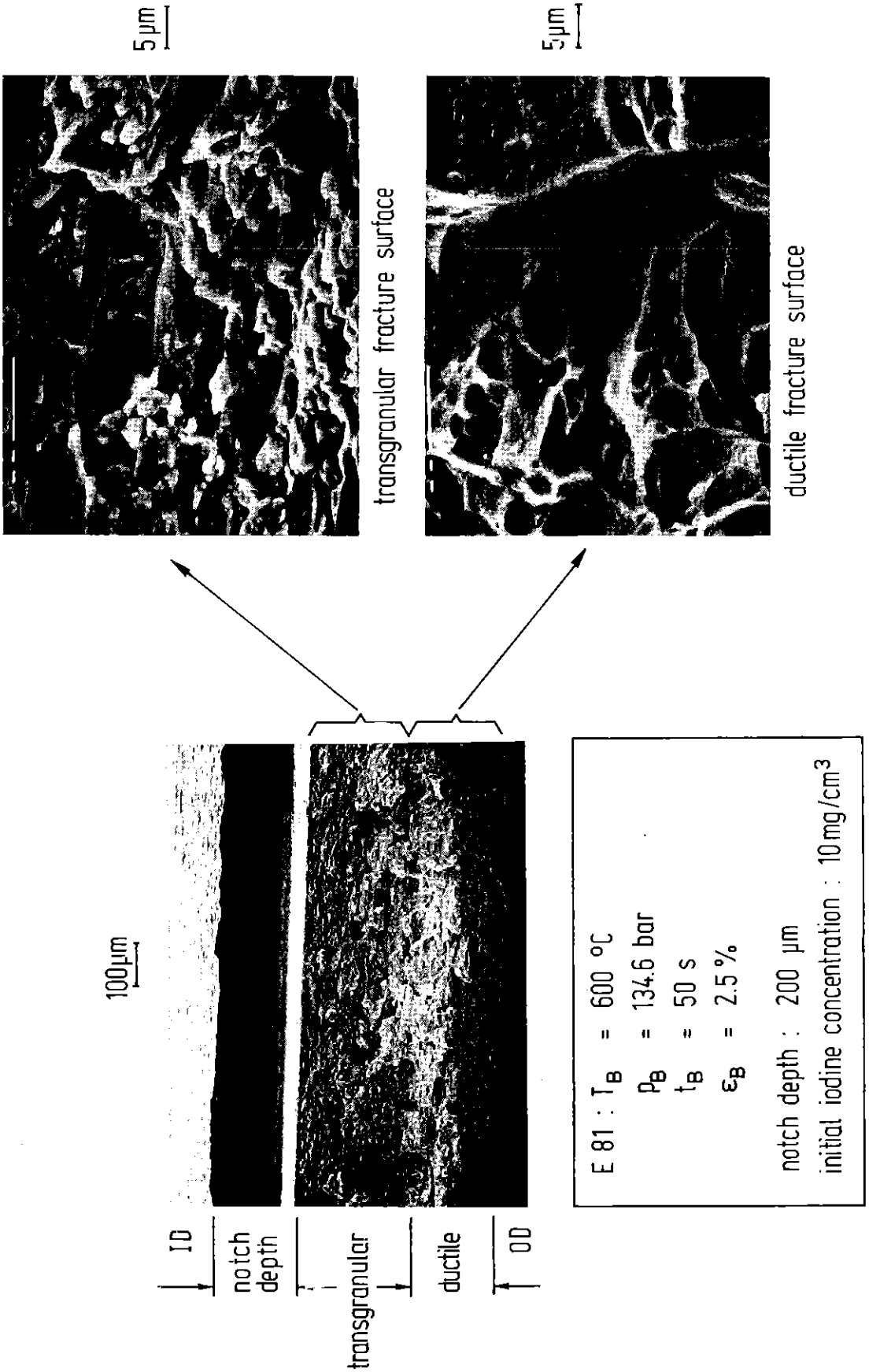

Fig.9: Zircaloy cladding tube fracture surface after failure under helium-iodine gas pressurization at 600°C.

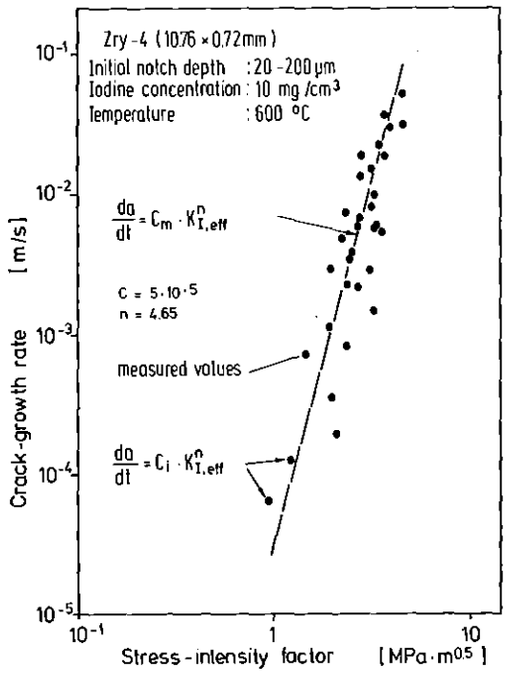

Fig.10: Iodine-induced corrosion-crack-growth rate as a function of the stress-intensity factor for Zircaloy-4 tubing at 600°C.

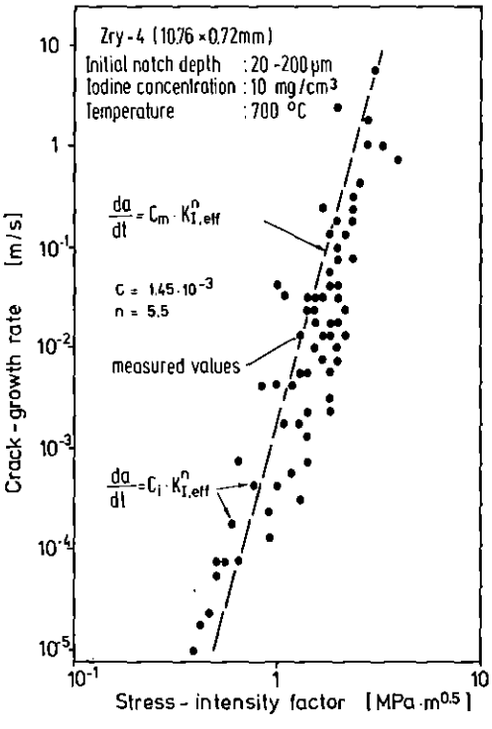

Fig.11: Iodine-induced corrosion-crack-growth rate as a function of the stress-intensity factor for Zircaloy-4 tubing at 700°C.

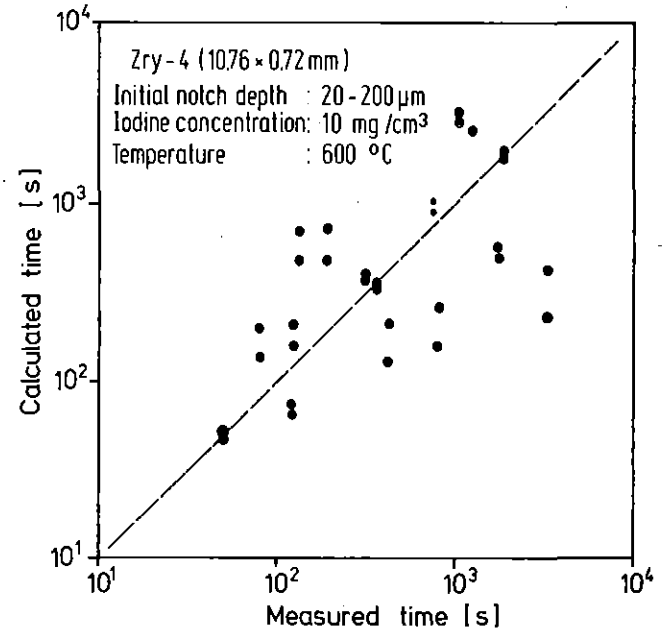

Fig.12: Comparison of the measured and calculated time-to-failure of preflawed Zircaloy-4 tubing at 600°C.

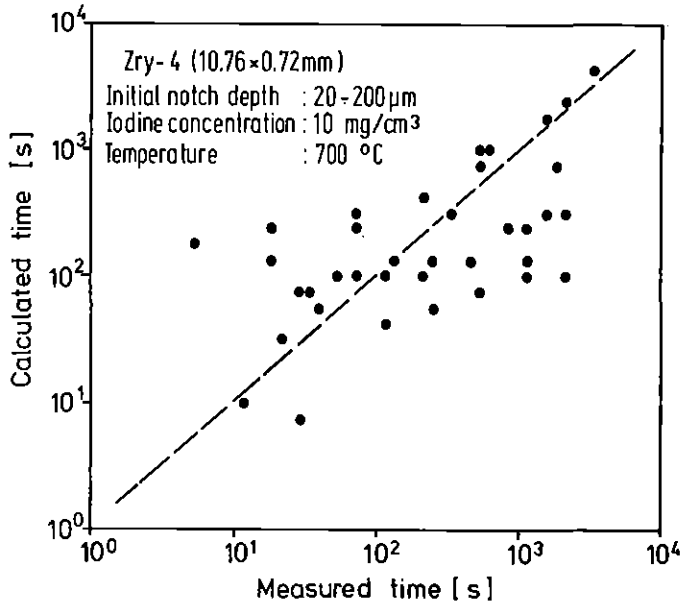

Fig.13: Comparison of the measured and calculated time-to-failure of preflawed Zircaloy-4 tubing at 700°C.